Supplementary Data

for the manuscript with the title of "*New type of crystallographic preferred orientation (CPO) of clinopyroxene in serpentinite*", written by *Jungjin Lee and Haemyeong Jung* (2024).

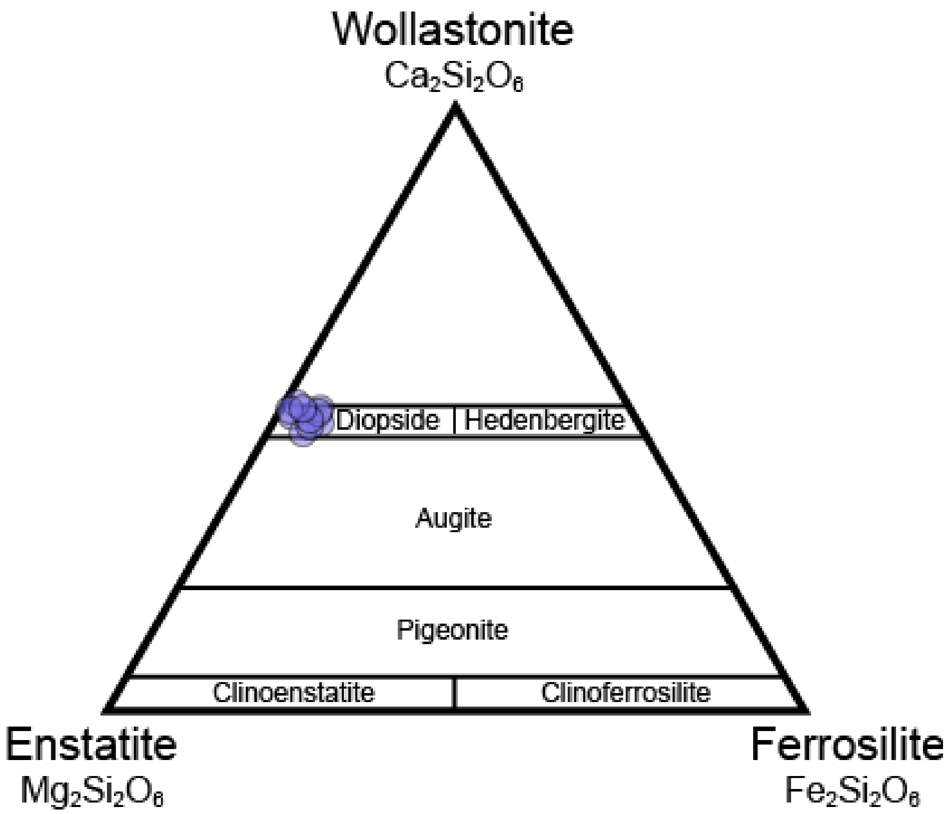

Supplementary Figure S1. Ternary classification diagram of the clinopyroxenes in the MSP serpentinite samples.

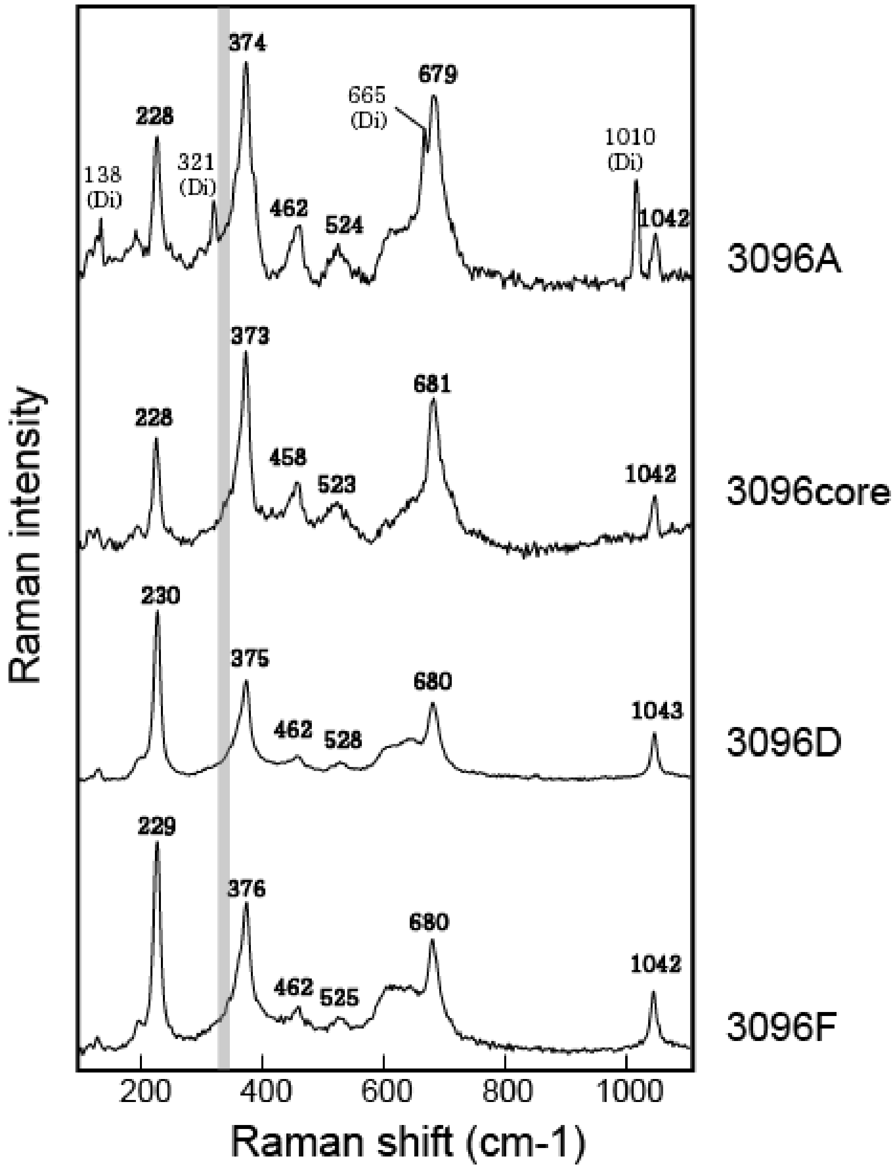

Supplementary Figure S2. Raman spectra of serpentine grains in the MSP diopside serpentinite samples (3096core, 3096D, 3096F and 3096A). Representative Raman spectra of samples were shown and they were almost identical. Strong peaks of 373–376 cm^{-1}, 680–681 cm^{-1}, and 1042–1043 cm^{-1} Raman shifts of antigorite and no peak around 350 cm^{-1} of lizardite/chrysotile (gray colored range) allowed the identification of antigorite in the samples. Raman spectra of sample 3096A included small peaks of adjacent diopside grains (Di) at the Raman shifts of 138, 321, and 665 cm^{-1}.

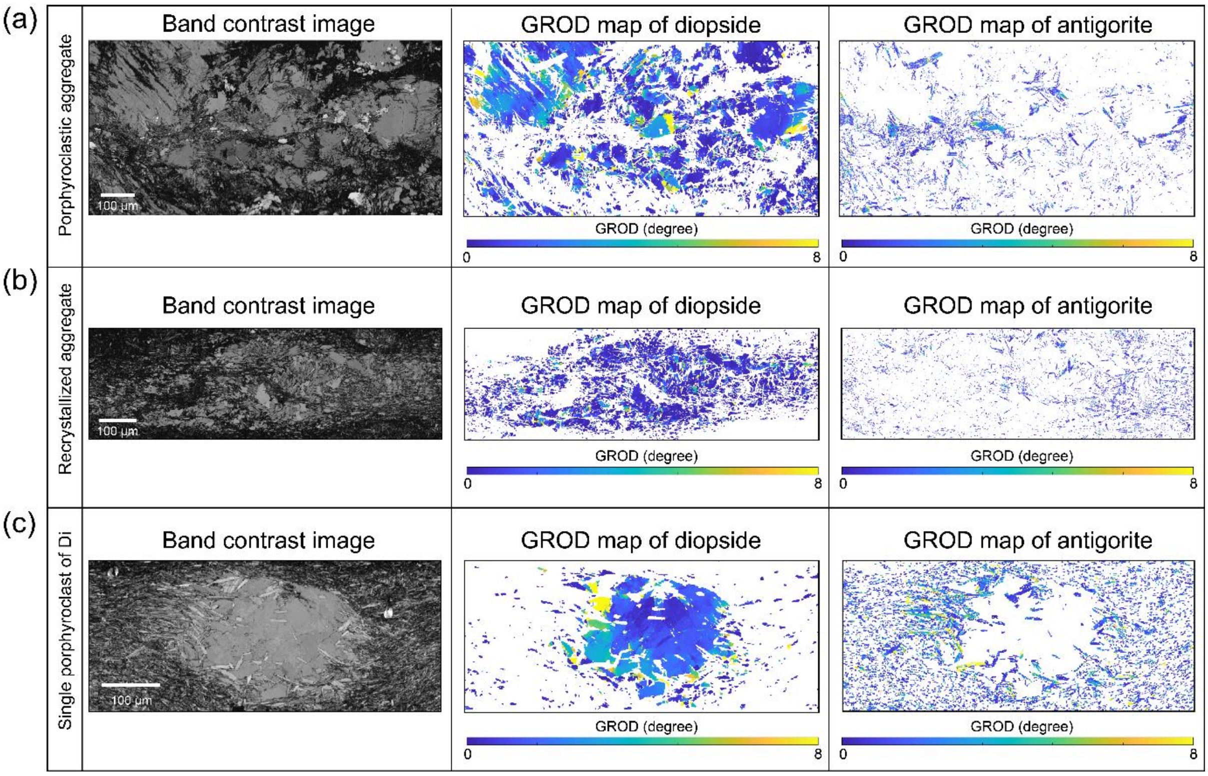

Supplementary Figure S3. Band contrast image and grain reference orientation deviation (GROD) map of diopside and antigorite in the representative areas of the MSP serpentinites. Three representative areas were selected based on grain sizes of diopside. **(a)** Porphyroclastic aggregate (sample 3096D), **(b)** recrystallized aggregate (sample 3096D), and **(c)** single porphyroclastic diopside and associated antigorites (sample 3096A). Vertical colorbars indicate the GROD values in degree (0 – 8 degrees). Porphyroclastic diopsides and large antigorite grains in (a) and (c) showed the high GROD values.

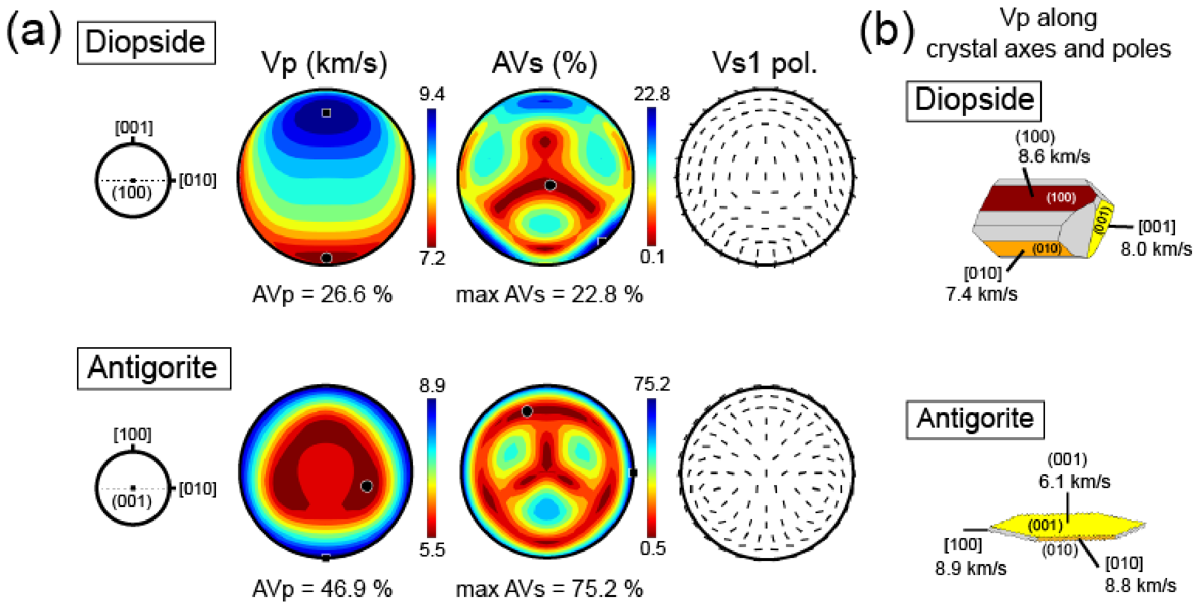

Supplementary Figure S4. Elastic anisotropy of single-crystal diopside and single-crystal antigorite. **(a)** Elasticity of single-crystal diopside and antigorite. P-wave velocity (Vp), S-wave seismic anisotropy (AVs), and fast S-wave polarization direction (Vs1 pol) were plotted. Elastic stiffness constants (C_{ij}) of diopside [1] and that of antigorite [2] were used, and mineral densities of diopside (3.26 g/cm^3) and antigorite (2.62 g/cm^3) were used. **(b)** P-wave velocities (Vp) along crystallographic axes and poles of diopside and antigorite. Representative crystallographic planes were colored (red; (100) plane, orange; (010) plane, yellow; (001) plane).

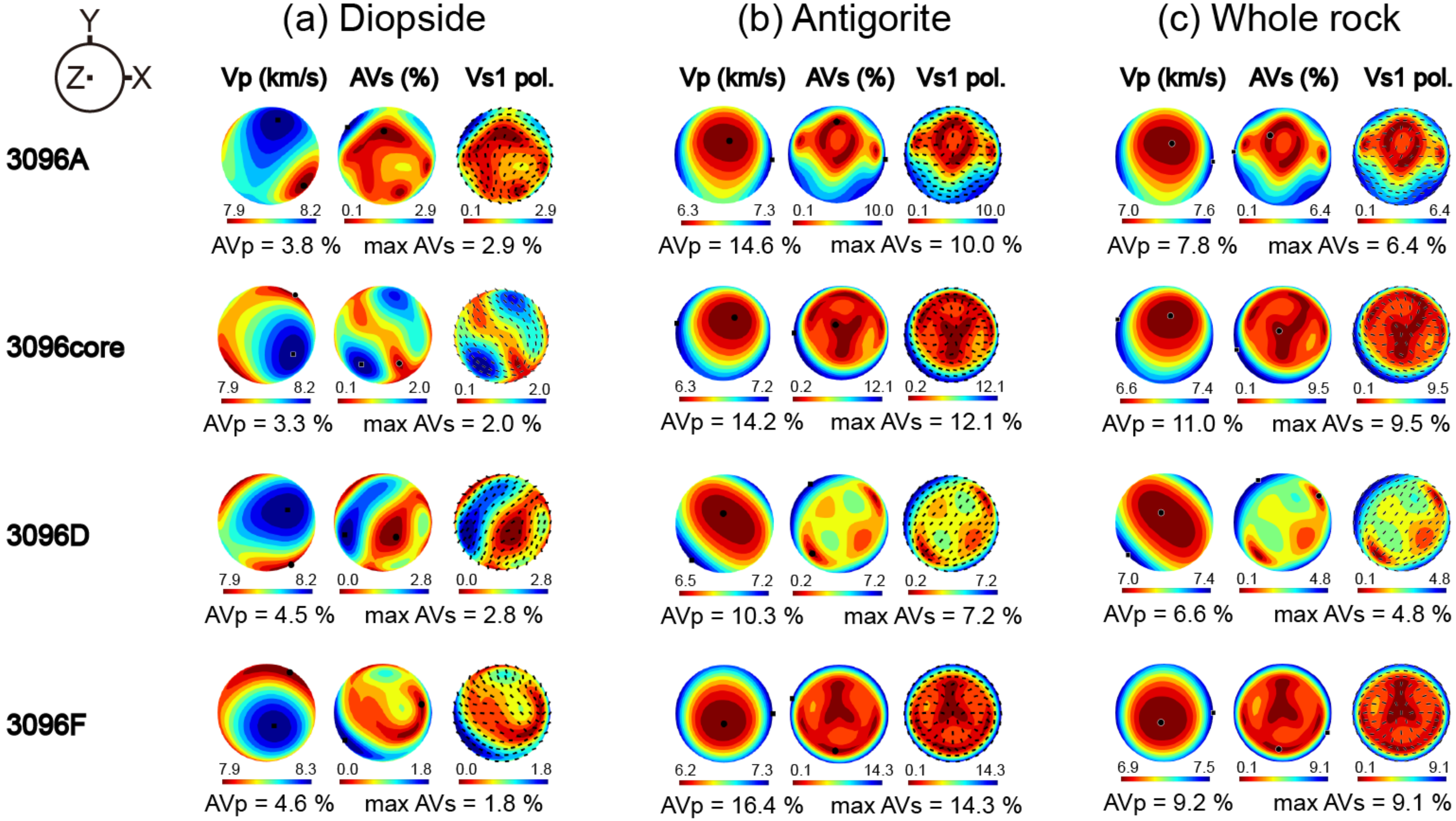

Supplementary Figure S5. (Caption in the next page)

Supplementary Figure S5. Seismic velocities and anisotropies of **(a)** diopside, **(b)** antigorite and **(c)** whole rock of the MSP diopside serpentinite samples. P-wave velocities (Vp), P-wave anisotropy (AVp), S-wave anisotropy (AVs) and fast S-wave polarization directions (Vs1 pol.) were plotted. Reference frame is plotted in the upper left for (a – c) where X-direction is parallel to the lineation and Z-direction is perpendicular to the X-Y plane which is parallel to the foliation. The seismic properties of whole rocks (diopside + antigorite) were calculated using the relative volume fraction between diopside and antigorite in each sample (*Table S1*).

Supplementary Table S1. Sample descriptions showing the mineral mode (volume percentage), large-area CPO type, and M-index (CPO strength) of antigorite and diopside in the MSP serpentinite samples.

Sample No.	Mineral mode (vol%)		CPO type		M-index	
	Atg	Di	Atg	Di	Atg	Di
3096A	69	31	(001) ⊥ S	(100) ⊥ S	0.05	0.06
3096core	84	16	(001) ⊥ S	(100) ⊥ S	0.05	0.03
3096D	77	23	(001) ⊥ S	(100) ⊥ S	0.04	0.07
3096F	73	27	(001) ⊥ S	(100) ⊥ S	0.07	0.05
Average	76	24			0.05	0.05

Atg: antigorite, Di: diopside, S: foliation.

Supplementary Table S2. Chemical compositions of diopside and antigorite in four serpentinite samples from the MSP.

Sample	3096A				3096core				3096D				3096F			
Minerals	Atg	Di_R	Di_P		Atg	Di_R	Di_P		Atg	Di_R	Di_P		Atg	Di_R	Di_P	
wt. %			core	rim			core	rim			core	rim			core	rim
SiO_2	40.9	54.2	51.3	51.8	41.4	55.4	50.4	50.8	41.0	55.0	51.2	54.5	43.4	55.1	50.5	51.0
TiO_2	0.0	0.0	0.6	0.6	b.d.	b.d.	0.9	1.1	0.0	0.0	0.9	0.6	b.d.	0.2	0.9	0.7
Al_2O_3	2.8	0.1	5.2	4.6	3.3	0.0	5.4	5.2	3.1	0.6	4.6	3.0	3.2	0.9	5.3	4.5
Cr_2O_3	0.3	0.1	1.1	1.1	0.3	0.0	1.1	1.2	0.6	0.3	0.9	0.6	0.5	b.d.	1.1	1.0
FeO *	5.8	1.4	2.9	2.9	5.7	1.3	3.0	2.8	5.6	2.0	3.0	2.5	5.6	2.9	3.1	3.1
MnO	0.1	0.1	0.1	0.1	0.1	0.1	0.1	0.0	0.1	0.1	0.1	0.1	0.1	0.2	0.0	0.1
MgO	36.3	18.5	15.8	15.8	35.8	17.8	15.1	15.2	35.8	17.1	16.0	16.5	37.3	16.0	14.7	15.9
CaO	0.0	25.3	22.3	22.8	0.0	26.2	22.9	22.9	0.1	24.5	22.2	23.8	0.1	24.4	23.2	22.4
Na_2O	0.0	0.1	0.7	0.6	0.0	0.1	0.7	0.7	0.0	0.2	0.6	0.4	0.0	0.2	0.6	0.5
K_2O	0.0	0.0	b.d.	b.d.	b.d.	0.0	b.d.	b.d.	0.0	0.0	0.0	b.d.	0.0	0.0	b.d.	b.d.
Total	86.2	99.8	99.8	100.2	86.5	100.9	99.6	99.8	86.3	99.8	99.4	101.9	90.3	99.8	99.3	99.2
#Mg	0.92	0.96	0.91	0.91	0.92	0.96	0.90	0.91	0.92	0.94	0.90	0.92	0.92	0.91	0.89	0.90

* Total Fe as FeO.

Atg, antigorite Di_R;, recrystallized small-sized diopside; Di_P, porphyroclastic diopside; b.d., below the detection limit.

Supplementary Table S3. Summary of the seismic anisotropies of antigorite, diopside, and bulk rocks of serpentinite samples.

	P-wave anisotropy (%)			Max S-wave anisotropy (%)		
	Atg	Di	Bulk	Atg	Di	Bulk
3096A	14.6	3.8	7.8	10.0	2.9	6.4
3096core	14.2	3.3	11.0	12.1	2.0	9.5
3096D	10.3	4.5	6.6	7.2	2.8	4.8
3096F	16.4	4.6	9.2	14.3	1.8	9.1
Average	13.9	4.1	8.7	10.9	2.4	7.5

Atg: antigorite, Di: diopside, Bulk: bulk rock.

References

1. Sang L, Bass JD. Single-crystal elasticity of diopside to 14 GPa by Brillouin scattering. *Physics of the Earth and Planetary Interiors* **228**, 75-79 (2014).

2. Bezacier L, Reynard B, Bass JD, Sanchez-Valle C, Van de Moortèle B. Elasticity of antigorite, seismic detection of serpentinites, and anisotropy in subduction zones. *Earth and Planetary Science Letters* **289**, 198-208 (2010).